11th World Congress on Computational Mechanics (WCCM XI)
5th European Conference on Computational Mechanics (ECCM V)
6th European Conference on Computational Fluid Dynamics (ECFD VI)
E. Oñate, J. Oliver and A. Huerta (Eds)

BLOCH THEOREM WITH REVISED BOUNDARY CONDITIONS APPLIED TO GLIDE PLANE AND SCREW AXIS SYMMETRIC, QUASI-ONE-DIMENSIONAL STRUCTURES

MAURIN F. * AND SPADONI A.†

* Laboratory of Wave Mechanics and Multi-Field Interactions (LOMI)
École Polytechnique Fédérale de Lausanne (EPFL)
1015 Lausanne, Switzerland
e-mail: florian.maurin@epfl.ch, web page: http://lomi.epfl.ch

†Laboratory of Wave Mechanics and Multi-Field Interactions (LOMI)
École Polytechnique Fédérale de Lausanne (EPFL)
1015 Lausanne, Switzerland
e-mail: alex.spadoni@epfl.ch, web page: http://lomi.epfl.ch

Key words: Bloch theorem, Boundary conditions, Discretized unit cell, Glide plane and screw axis symmetries.

Abstract. Bloch theorem provides a useful tool to analyze wave propagation in periodic systems. It has been widely used in physics to obtain the energy bands of various translationally-periodic cristals and with the advent of nanosciences like nanotubes, it has been extended to additional symmetries using group theory. However, this work is restricted to homogenous equations. For complexe problems, as engineering structures, the peridic unit cell are often discretized and Bloch method is restricted to translational periodicity.

The goal of this paper is to generalize the direct and transfer propagation Bloch method to structures with in glide plane or screw axis symmetries by deriving appropriate boundary conditions. Dispersion relations for a set of problems is then given and compared to results from the classical method, if available. It is found that (i) the dispersion curves are easier to interpret, (ii) the computational cost and error is reduced, and (iii) revisited Bloch method is applicable to structures that do not possess purely-translational symmetries for which the classical method is not applicable.

1 Introduction

Wave propagation in structures is used in a large range of applications such as non-destructive evaluation for structural health monitoring [1] and imaging [2]. In the case

of translational periodic structures, Bloch theorem is used to obtain the behavior of an infinite medium from the analysis of a single unit cell [3]. It can be used for example to get the electronic band gaps structures in crystals [4] as well as dispersion relation of railways [5]. However, in the presence of symmetries other than translation, Bloch theorem in its original form cannot be used.

These challenges are being addressed with two approaches: in modern physics, Hamiltonian systems with analytical or simple potentials can be analyzed via group theory [6], and find applications among nanotubes, nonoribbons, DNA, proteins or polymers structures. The presence of symmetries allows significant simplification and reduced computation cost. The advent of the finite element method (FEM), originally developed for engineering problems, introduce the ability to analyze highly complex systems. As a result, FEM is now commonly employed. The presence of symmetries in such formulations is handled by periodic-boundary conditions. For translation symmetries, the employment of Bloch theorem is hence a natural extension of FE, and significant research has been devoted to analyzing wave propagation in infinite system following two different approaches: Assuming harmonic waves (propagating without attenuation), the system can be reduced to an eigenvalue problem for which, the frequencies are the solutions. This method, referred as direct, has been especially used by Phani [7] who study band structures of honeycomb lattices in the Irreducible Brillouin Zone (IBZ). An alternative to this method consist on using the transfer matrix approach [8], which yields the propagation and attenuation part of the wave at a given frequency. Initially available for one-dimensional problems, this technique has been extended to 2D problems for portions of the IBZ [9], and more recently for the entire IBZ [10, 11]. Both methods however are not immediately extended to systems with symmetries other than translation.

In this paper, we derive appropriate boundary conditions for glide-plane and screw-axis symmetric systems for both the direct and transfer-matrix approaches. It follows our previous work on the dispersion of a post-buckled beam [12], a structure which is glide symmetric. In [13], a glide symmetric warren truss is considered without mentioning the symmetry. In the literature, to the best of our knowledge, only helical waveguides with constant cross sections as multi-wires have been analyzed with the Bloch method [1]. However, our method differs in the choice of the reference coordinate system and it is generalized to the full screw-symmetric group.

This paper is organized as follows. In Sec. 2, we propose appropriate boundary conditions which reduce unit-cell bases on translation symmetry to simplified subcells according to the additional symmetries. We demonstrate that these boundary conditions leave the eigenvalues of the dynamic equation unchanged, in accordance with the present symmetries. We then demonstrate in Sec. 3 the applicability of the proposed method in a set of quasi-one dimensional problems, with respect to wave propagation.

2 Reduced Bloch Theorem

Wave propagation in periodic structures can be investigated through the analysis of a unit cell and the application of Bloch theorem [3, 7, 9]. The motion of a linear, periodic domain resulting from uniaxial wave propagation may be expressed as follows:

$$\boldsymbol{d}_n = \boldsymbol{d}_0(\mu(\omega))e^{\mu n}, \tag{1}$$

where $\boldsymbol{d}_n$ denotes the displacement vector of cell n within the periodic assembly, and $\boldsymbol{d}_0$ is the displacement vector within the reference cell. The propagation constant μ is a complex number ($\mu = \delta + \mathrm{i}\epsilon$, $\mathrm{i} = \sqrt{-1}$) where the real and imaginary parts represent respectively the attenuation and phase constants. Given the periodicity, the propagation constant μ is equal to the wave number κ multiplied by the spatial period L such that $\mu = L\kappa$. The governing equation is:

$$\mathbf{M}\ddot{\boldsymbol{d}} + \mathbf{K}\boldsymbol{d} = \boldsymbol{f}, \tag{2}$$

where $\boldsymbol{d}$ and $\boldsymbol{f}$ are the displacement and forces defined by $\boldsymbol{d} = \{\boldsymbol{d}_L^T\ \boldsymbol{d}_I^T\ \boldsymbol{d}_R^T\}^T$ and $\boldsymbol{f} = \{\boldsymbol{f}_L^T\ \boldsymbol{f}_I^T\ \boldsymbol{f}_R^T\}^T$. The subscripts $(\,)_L$, $(\,)_I$ and $(\,)_R$ respectively denote the left, internal and right displacements/forces of a unit cell. Assuming harmonic motion, Eq. (2) gives:

$$\mathbf{D}(\omega)\boldsymbol{d} = \begin{bmatrix} \mathbf{D}_{LL} & \mathbf{D}_{LI} & \mathbf{D}_{LR} \\ \mathbf{D}_{IL} & \mathbf{D}_{II} & \mathbf{D}_{IR} \\ \mathbf{D}_{RL} & \mathbf{D}_{RI} & \mathbf{D}_{RR} \end{bmatrix} \boldsymbol{d} = \boldsymbol{f}. \tag{3}$$

where $\mathbf{D}(\omega) = [\mathbf{K} - \omega^2\mathbf{M}]$ is the dynamic stiffness matrix.

The unit cell shown in Fig. 1a is composed of two arrows and reproduces the infinite structure by translation symmetries. The same unit cell however has an intrinsic glide-reflection symmetry (axial-reflection plus translation). In the same manner, the unit cell of Fig. 1c represents a circle with five arrows and can be obtained from a single arrow using screw-axis symmetries. In both cases, glide or screw symmetries can be exploited and the unit cell of Fig. 1b or Fig. 1d are respectively used instead.

To distinguish the different variables defined for the reduced and full unit cell, the respective superscripts $\widehat{(\,)}$ and $\widetilde{(\,)}$ are used. p is the number of intrinsic reduced unit cells contained by period of translation ($p = 2$ for glide symmetry).

Using the full period (Figs. 1a,c) and imposing periodicity conditions on the generalized displacement and equilibrium conditions on the generalized forces yields:

$$\begin{Bmatrix} \boldsymbol{d}_L \\ \boldsymbol{f}_L \end{Bmatrix} = e^{-\widetilde{\mu}} \begin{Bmatrix} \widetilde{\boldsymbol{d}}_R \\ -\widetilde{\boldsymbol{f}}_R \end{Bmatrix}, \tag{4}$$

where $\widetilde{\mu} = pL\mathrm{Im}(\kappa)$ and L is the period length of the reduced unit cell. The equivalent relation for the reduced period (Fig. 1b) is:

$$\begin{Bmatrix} \boldsymbol{d}_L \\ \boldsymbol{f}_L \end{Bmatrix} = e^{-\widehat{\mu}} \begin{Bmatrix} \widehat{\boldsymbol{d}}_R \\ -\widehat{\boldsymbol{f}}_R \end{Bmatrix} = e^{-\widehat{\mu}} \begin{bmatrix} R_o & \mathbf{0} \\ \mathbf{0} & R_o \end{bmatrix} \begin{Bmatrix} \widetilde{\boldsymbol{d}}_R \\ -\widetilde{\boldsymbol{f}}_R \end{Bmatrix}, \tag{5}$$

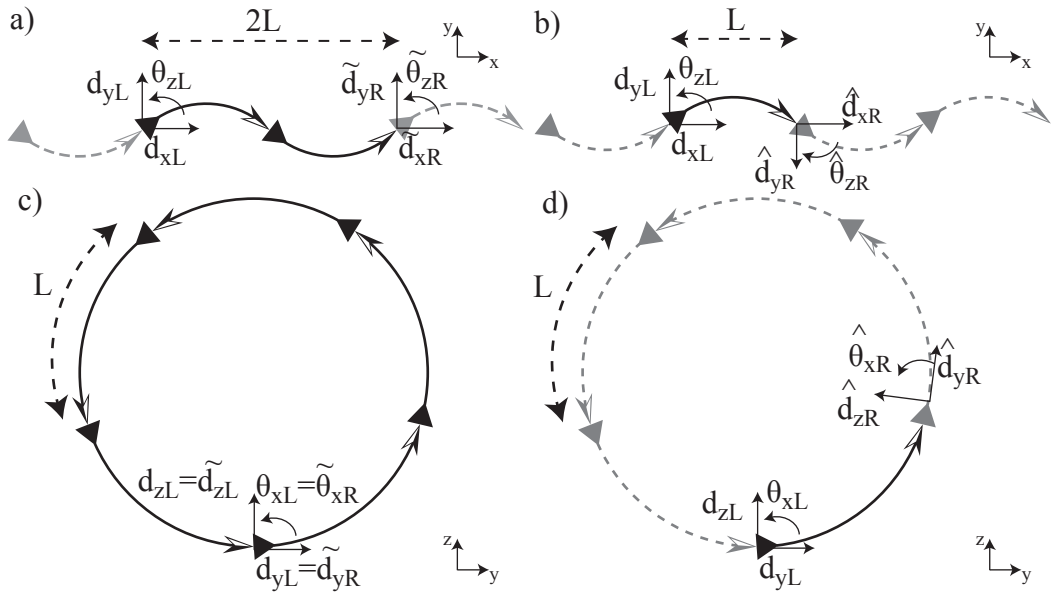

Figure 1: Unit cell in full black line in terms of the classical (a, c) and revisited (b, d) Bloch theorem taking into account 2D glide reflection (b) or screw (d) symmetries. Figures are shown in the plane but a third direction can exist.

where $\mathbf{0}$ is the zero matrix, $\widehat{\mu} = \widetilde{\mu}/p$, and $R_o = I_o \otimes R$, with $\otimes$ the Kronecker product. R is an orthogonal ($R^{-1} = R^T$) change of basis matrix from $\widetilde{\boldsymbol{d}}_R$ to $\widehat{\boldsymbol{d}}_R$ denoted by R_y and R_θ respectively in the case of glide symmetries of plane (x, z) (Fig. 1b) and screw symmetries (Fig. 1d) such that for a wave propagating in the x direction R is:

$$R_y = \begin{bmatrix} 1 & 0 & 0 & 0 & 0 & 0 \\ 0 & -1 & 0 & 0 & 0 & 0 \\ 0 & 0 & 1 & 0 & 0 & 0 \\ 0 & 0 & 0 & 1 & 0 & 0 \\ 0 & 0 & 0 & 0 & -1 & 0 \\ 0 & 0 & 0 & 0 & 0 & -1 \end{bmatrix}, \quad R_\theta = \begin{bmatrix} 1 & 0 & 0 & 0 & 0 & 0 \\ 0 & \cos\theta & \sin\theta & 0 & 0 & 0 \\ 0 & -\sin\theta & \cos\theta & 0 & 0 & 0 \\ 0 & 0 & 0 & 1 & 0 & 0 \\ 0 & 0 & 0 & 0 & \cos\theta & \sin\theta \\ 0 & 0 & 0 & 0 & -\sin\theta & \cos\theta \end{bmatrix}. \quad (6)$$

These matrices are given for 3D elements with 6 degrees of freedoms (dofs) per node (3 displacements plus 3 rotations such that $[d_x\ d_y\ d_z\ \theta_x\ \theta_y\ \theta_z]$). For example, if the formulation is beam element in the plane (i.e. Fig. 1a), only the first, second and last rows/columns of R_y are kept.

The angle θ in the screw symmetry is the angle of rotation but is also the period of the propagation constant. Indeed, since the period of the $\widetilde{\mu}$ is 2π, the period of $\widehat{\mu} = \widetilde{\mu}/p$ is $2\pi/p = \theta$. For glide symmetry, the reduced period is π.

2.1 Direct method

Using Eq. (5), $\widetilde{\boldsymbol{d}} = \{\boldsymbol{d}_L^T \ \boldsymbol{d}_I^T \ \widetilde{\boldsymbol{d}}_R^T\}^T$ can be expressed in terms of a reduced displacement vector $\boldsymbol{d}^{(r)} = \{\boldsymbol{d}_L^T \ \boldsymbol{d}_I^T\}^T$:

$$\widetilde{\boldsymbol{d}} = \begin{bmatrix} I_{do} & \mathbf{0} \\ \mathbf{0} & I_{di} \\ R_o^T e^{\widehat{\mu}} & \mathbf{0} \end{bmatrix} \boldsymbol{d}^{(r)} = \widehat{Z}\boldsymbol{d}^{(r)}, \tag{7}$$

where I is an identity matrix of size defined by subscripts; do and di are the number of dofs by node d multiply by the number of external o and internal i node, respectively. Assuming the propagating wave without attenuation ($\widehat{\mu} = i\widehat{\epsilon}$) and no internal forces ($\boldsymbol{f}_I = \mathbf{0}$), and substituting Eq. (7) into Eq. (3) then multiplying both sides by $\widehat{Z}^H$, where H denotes the conjugate transpose, gives:

$$\widehat{\mathbf{D}}^{(r)}(\omega, \widehat{\mu})\boldsymbol{d}^{(r)} = \mathbf{0}, \tag{8}$$

where $\widehat{\mathbf{D}}^{(r)}(\omega, \widehat{\mu}) = \widehat{Z}^H\widehat{\mathbf{D}}(\omega)\widehat{Z}$. Given the periodicity of the medium, $\widehat{\epsilon}$ =Im$(\widehat{\mu}) \in [-\pi \ \pi]$, and associated values of ω are found by solving the eigenvalue problem of Eq. (8).

2.2 Inverse method

Instead of fixing the wave number and looking for the associated frequency, one can fix the frequency and compute the propagation constant $\widehat{\mu}$ for 1D problems [8]. In absence of internal forces, Eq. (3) can be recast as:

$$\widehat{\mathfrak{D}}(\omega) \begin{Bmatrix} \boldsymbol{d}_L \\ \widetilde{\boldsymbol{d}}_R \end{Bmatrix} = \begin{bmatrix} \widehat{\mathfrak{D}}_{LL} & \widehat{\mathfrak{D}}_{LR} \\ \widehat{\mathfrak{D}}_{RL} & \widehat{\mathfrak{D}}_{RR} \end{bmatrix} \begin{Bmatrix} \boldsymbol{d}_L \\ \widetilde{\boldsymbol{d}}_R \end{Bmatrix} = \begin{Bmatrix} \boldsymbol{f}_L \\ \widetilde{\boldsymbol{f}}_R \end{Bmatrix}, \tag{9}$$

with $\widehat{\mathfrak{D}}_{XY} = \widehat{D}_{XY} - \widehat{D}_{XI}\widehat{D}_{II}^{-1}\widehat{D}_{IY}$ ($\{(\ )_X, (\ )_Y\} \in \{(\ )_L, (\ )_R\}$). Eq. (9) can be rearranged to define a relation between opposite sides of the unit cell:

$$\begin{Bmatrix} \widetilde{\boldsymbol{d}}_R \\ -\widetilde{\boldsymbol{f}}_R \end{Bmatrix} = \begin{bmatrix} -\widehat{\mathfrak{D}}_{LR}^{-1}\widehat{\mathfrak{D}}_{LL} & \widehat{\mathfrak{D}}_{LR}^{-1} \\ \widehat{\mathfrak{D}}_{RR}\widehat{\mathfrak{D}}_{LR}^{-1}\widehat{\mathfrak{D}}_{LL} - \widehat{\mathfrak{D}}_{RL} & -\widehat{\mathfrak{D}}_{RR}\widehat{\mathfrak{D}}_{LR}^{-1} \end{bmatrix} \begin{Bmatrix} \boldsymbol{d}_L \\ \boldsymbol{f}_L \end{Bmatrix} = \widehat{T} \begin{Bmatrix} \boldsymbol{d}_L \\ \boldsymbol{f}_L \end{Bmatrix}, \tag{10}$$

where $\widehat{T}$ is the transfer matrix. Combining Eqs. (5) and (10) gives:

$$\left[[I_2 \otimes R_o]\, \widehat{T} - I_{do} e^{\widehat{\mu}} \right] \begin{Bmatrix} \boldsymbol{d}_L \\ \boldsymbol{f}_L \end{Bmatrix} = \mathbf{0}. \tag{11}$$

Eq. (11) is an eigenvalue problem which gives $2do$ complex conjugate eigenvalues $e^{\widehat{\mu}}$ corresponding to frequency ω.

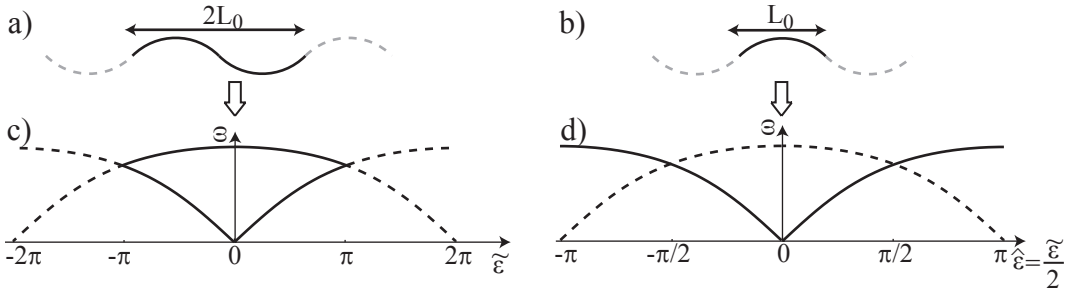

Figure 2: Repercussions of glide symmetry on dispersion relations of post-buckled structures. Full (a) and revisited (b) unit cells with respective band structures (c) and (d). Full lines in (c, d) denote the solution in the first Brillouin zone (BZ), while dashed-black lines denote solutions in the second BZ.

3 Results

In this section, a set of different examples is given to compare the classical Bloch theorem to its revisited version. For beam elements, the following notation and numerical values are used in this section: the beam cross-section is square of thickens $t = 1$ mm, area $A = t^2$ and area-moment of inertia $I = t^4/12$; $E = 200$ GPa is the Young modulus, and the density is $\rho = 8100$ Kg m^{-3}.

3.1 Post-buckled beam

A post-buckled beam (Figs. 2a,b) is an example of geometry with glide symmetries which has been studied in [12]. In the present case, we restrict ourselves to the global trend of the curve to compare the classical Bloch theorem to its revisited version with the direct method. For more details on the dispersion of post-buckled structures with interpretations of the different modes, including a analyze of the influence of pre-stress, type of supports, and buckling level, please refer to [12].

The band structure for the translational unit cell (Fig. 2c) gives dispersion curves belonging to the interval $\widetilde{\epsilon} = 2L\text{Im}(\kappa) = [-\pi\ \pi]$. But $\widetilde{\epsilon}$ is not restricted to this interval and the full dispersion is obtained by shifting the curves in full line by $2q\pi$ ($q \in \mathbb{N}$) resulting in the dashed lines in Fig. 2c [3]. Dashed lines however do not provide any additional information given the periodicity of the dispersion relations. In the dispersion from the revisited Bloch version (Fig. 2d), the interval is still $\widehat{\epsilon} = L\text{Im}(\kappa) = [-\pi\ \pi]$ but the period of the propagation constant is π. When full lines are shifted by the period $q\pi$, new roots appear in the interval $\widehat{\epsilon} = [-\pi\ \pi]$ (dashed line) recovering the dispersion of the full periodicity (Fig. 2c) using $\widehat{\epsilon} = \widetilde{\epsilon}/2$. One comment is due comparing the full line curves of Fig. 2c to Fig. 2d. In Fig. 2c, it is not clear if the two branches ($\widetilde{\epsilon} \geq 0$) of the dispersion curves are due to the same phenomenon, while this is clear in Fig. 2d due to the continuity of the curve. Finally, the revisited Bloch theorem produces band structures that are easier to interpret, as we emphasize in the next example.

3.2 Helix in a plane

In this example, dispersion of a wave propagating in a plane helix (2D) is analyzed. Modeling the helix by a slender curved beam of radius r, an analytical dispersion equation relating the wave number κ to the frequency ω can be derived from beam theory [14]:

$$\kappa^6 - \left(\kappa_0^2 + \frac{2}{r^2}\right)\kappa^4 - \left(\beta^4 + \frac{\kappa_0^2}{r^2} - \frac{1}{r^4}\right)\kappa^2 + \left(\kappa_0^2 - \frac{1}{r^2}\right)\beta^4 = 0, \tag{12}$$

where $\kappa_0^2 = \omega^2 \frac{\rho}{E}$ and $\beta^4 = \omega^2 \frac{\rho A}{EI}$. The goal of this part is to recover Eq. (12) using FEM and Bloch theorem. For this purpose, a portion of 360° of the infinite helix corresponding to the periodicity by translation is discretized using p beam finite elements [15]. This "open ring" is used as a unit cell for the classical Bloch theorem and dispersion curves are shown in Figs. 3a,b for the direct and inverse method. The helix is screw symmetric as well with a periodicity that can be reduced to an infinitesimally small portion. However, in the present case, since we are using FE, the minimum size for the screw periodicity is one beam element. Using this reduced unit cell, the revisited Bloch theorem can be used choosing the rotation matrix R_θ (Eq. (6)) with $\theta = 360°/p$, and dispersion curves are shown in Figs. 3c,d for the direct and inverse method. A discussion on the different modes interpretations can be found in [14]. For a comparison between the classical (Figs. 3a,b) and the revisited (Figs. 3c,d) Bloch theorem, three main comments are in order:

- Band structures resulting from the revisited Bloch theorem are easier to interpret. Indeed in Fig. 3a for example, the full line in folding describing the dispersion in the first Brillouin zone (BZ) or its extension to other BZ (dashed lines) are both not clear compared to the dispersion obtained with the revisited Bloch theorem (Fig. 3c).

- Results from the revisited Bloch theorem are more accurate. Indeed, focusing on Fig. 3b, the branch with the largest real part is wrong for $\omega/\omega_0 \geq 3$ and spurious results are present in the imaginary part for $\omega/\omega_0 \approx 8$ and $\omega/\omega_0 \geq 10$. This is due to the fact that the matrix to be inverted in the classical Bloch theorem is p ($p = 64$ in Fig. 3) times larger, increasing the probability to get computational errors.

- The last advantage arising from the matrix size is computation time. Indeed the eigenvalue problem or the matrices to invert are p times smaller, respectively in the direct and inverse method. Moreother the computation cost increase in the classical Bloch theorem when the discretization is refined (p increase) whereas it remain unchanged for the revisited Bloch theorem as shown in Table. 1.

In addition to these advantages, we conclude by emphasizing that the plane helix is a very particular type of screw symmetry since the translation is null. This means that the only way to get a dispersion direction is along the curvilinear beam and so $\widehat{\mu} = \frac{\widetilde{\mu}}{p} = \frac{2\pi r}{p}\kappa$. In general, helixes are 3D structures and due to the fact that Bloch theorem is restricted

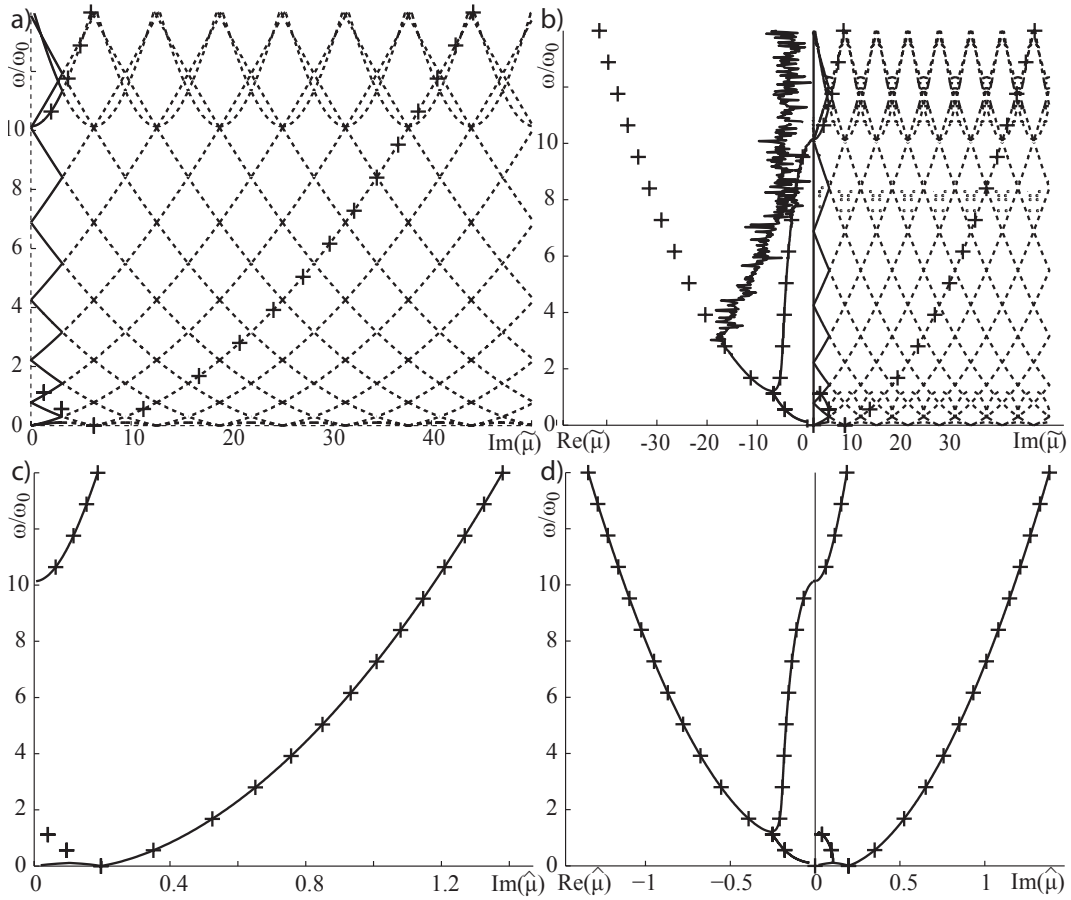

Figure 3: Dispersion relation of the plane helix computed with the classical (a, b) and revisited (c, d) Bloch theorem using the direct (a, c) and indirect (b, d) method and a discretization of $p = 64$. Full lines denote the solution in the first BZ, while dashed lines denote solutions in the others BZ. The + are results from the analytical dispersion (Eq. (12)). These figures are plotted for $r = 10t$ as in [14] and $\omega_0 = \pi^2\sqrt{E/\rho}$.

Table 1: Computation time of the revisited and classical Bloch theorem for a set of several levels of discretization with p the number of element by portion of 360° of the helix.

Computation time (s)	Revisited	Classical			
p	$\forall p$	4	16	64	256
Direct method	1	14	21	111	2024
Inverse method	0.22	0.40	0.54	1.09	3.15

to quasi-one dimensional structures, the dispersion is usually obtained along the screw axis, as shown in the next example.

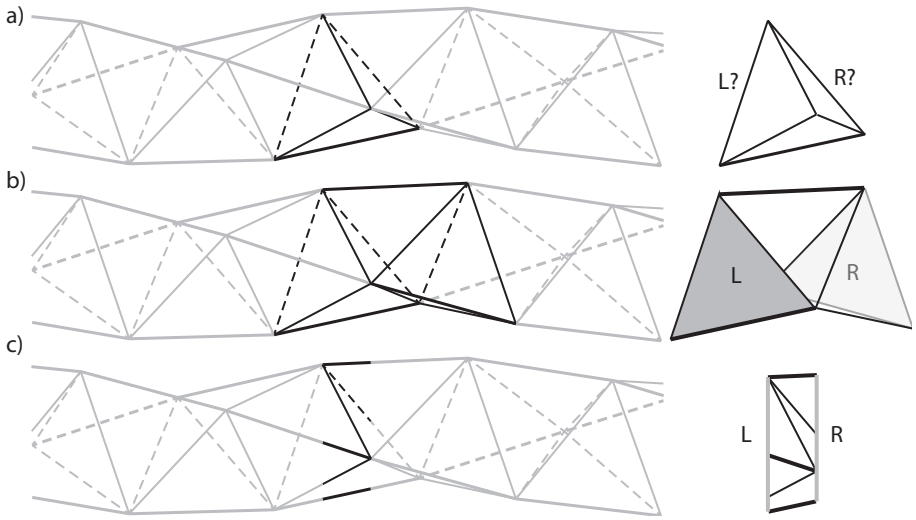

Figure 4: Tetrahelix structures with different unit cells: a single tetrahedron (a), an assembly of three tetrahedra (b) and a cut of length h_0 along and perpendicular to the screw axis (c). The letters "L" and "R" denotes the left and right sides of the unit cell, if existing.

3.3 The Boerdijk-Coxeter helix (tetrahelix)

The Boerdijk-Coxeter helix also called tetrahelix is a particular helical structure built from stacking of tetrahedra (Fig. 4a). The tetrahelix is a screw symmetric structure: a translation along its axes by $h_0 = a/\sqrt{10}$ (a the length of a tetrahedron edges) coupled to a rotation of $\theta_0 = \arccos(-2/3)$ [16]. Since θ_0 is not a fraction of π, the tetrahelix does not possess pure translational symmetry and it is an example of structures where only the revisited Bloch theorem can be applied; the classical Bloch method cannot be employed.

The first step in Bloch theorem is to define the unit cell and a first guess would be to use one tetrahedron (Figs. 4a). However, the tetrahedron possesses four sides, all linked together, meaning that some nodes are shared by both the right and left sides which is not possible (wave number equal to zero). To overcome this problem, instead of using one tetrahedron as a unit cell, a possibility is to use an assembly of three of them as shown in Figs. 4b, and taking the rotation matrix R_θ (Eq. (6)) defined with $\theta = 3\theta_0$. The dispersion obtained from the direct method is shown in Fig. 5a in full lines. Beside a physical interpretation of the results which is not of interest in this paper, we notice that some curves at their extremities ($\widehat{\mu} = 0$ or $\widehat{\mu} = \pi/3$) are joined (see zooms). Since this observation is similar to previous ones (Figs. 2c and 3a), we expect the unit cell to be reducible by three, to match the period of the screw symmetry. Indeed, this reduction can be archived taking a portion of the helix of length h_0 cut along and perpendicular to the screw axis as shown in Figs. 4c. The new dispersion relation is shown in Fig. 5b and as expected, the superposition of Fig. 5a and Fig. 5b overlaps perfectly.

Finally, note that in Fig. 5, there is a particular point for which $\omega = 0$ with $\widehat{\mu} = \theta_0 \neq 0$ (Fig. 5b). This is not the result of a wave propagating without frequency but this is

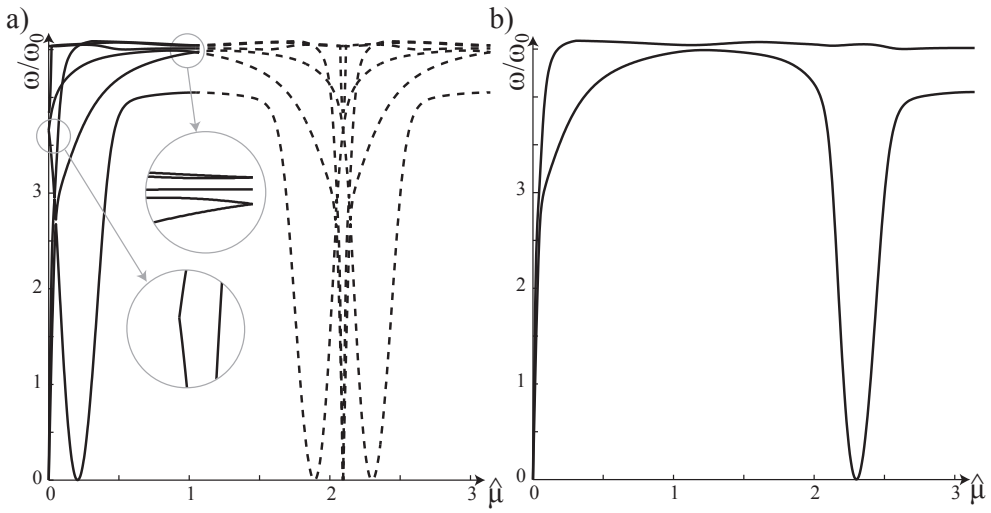

Figure 5: Dispersion relation of the tetrahelix from the revisited Bloch theorem with the direct method of the unit cell shown in Fig. 4b (a) and Fig. 4c (b). Full lines denote the solution in the first BZ, while dashed lines denote solutions in the others BZ. Dispersion curves are obtained along the screw axis in terms of $\widehat{\mu} = h_0\kappa$ and with the following parameters: $a = 0.1$ m and $\omega_0 = \sqrt{EA/\rho/a^2}$.

consequence of the fact that the screw angle is not a fraction of π. As it will be shown in an upcoming paper, it is possible to give an alternative representation of Fig. 5 where all dispersion curves start from the position $\omega = \mu = 0$.

4 Conclusions

In this paper, we revisit boundary conditions in Bloch theorem to account for glide and screw symmetries. Both the direct and the transfer version are addressed. After comparing dispersion relation resulting from the classical and revisited method for a set of different problem, it is found that (i) the dispersion curves are easier to interpret, (ii) the computational cost and error is reduced, and (iii) the revisited Bloch method is applicable to structures that do not possess purely-translational symmetries for which the classical method is not applicable.

REFERENCES

[1] F. Treyssède. Numerical investigation of elastic modes of propagation in helical waveguides. *The Journal of the Acoustical Society of America*, 121(6):3398–408, 2007.

[2] A. Ishimaru. *Wave propagation and scattering in random media*. Number vol. 1. Elsevier Science, 2013.

[3] L. Brillouin. *Wave Propagation in Periodic Structures: Electric Filters and Crystal Lattices*. 2003.

[4] C. Kittel. *Introduction to Solid State Physics*, volume 2004. 2004.

[5] D. J. Mead. Wave Propagation in Continuous Periodic Structures: Research Contributions From Southampton, 19641995. *Journal of Sound and Vibration*, 190(3):495–524, 1996.

[6] O. O. Kit, L. Pastewka, and P. Koskinen. Revised periodic boundary conditions: Fundamentals, electrostatics, and the tight-binding approximation. *Physical Review B*, 84(15):155431, 2011.

[7] A. S. Phani, J. Woodhouse, and N. A. Fleck. Wave propagation in two-dimensional periodic lattices. *The Journal of the Acoustical Society of America*, 119(4):1995, 2006.

[8] F. Romeo and A. Paolone. Wave propagation in three-coupled periodic structures. *Journal of Sound and Vibration*, 301(3-5):635–648, 2007.

[9] A. Spadoni, M. Ruzzene, and K. Cunefare. Vibration and Wave Propagation Control of Plates with Periodic Arrays of Shunted Piezoelectric Patches. *Journal of Intelligent Material Systems and Structures*, 20(8):979–990, 2009.

[10] M. Collet, M. Ouisse, M. Ruzzene, and M. N. Ichchou. FloquetBloch decomposition for the computation of dispersion of two-dimensional periodic, damped mechanical systems. *International Journal of Solids and Structures*, 48(20):2837–2848, 2011.

[11] F. Farzbod and M. J. Leamy. Analysis of Blochs Method and the Propagation Technique in Periodic Structures. *Journal of Vibration and Acoustics*, 133(3):031010, 2011.

[12] F. Maurin and A. Spadoni. Wave dispersion in periodic post-buckled structures. *Submited to Journal of Sound and Vibration, under review*, 2014.

[13] E. G. Karpov, D. L. Dorofeev, and N. G. Stephen. Characteristic solutions for the statics of repetitive beam-like trusses. *International Journal of Mechanical Sciences*, 44(7):1363–1379, 2002.

[14] J. F. Doyle. *Wave Propagation in Structures: Spectral Analysis Using Fast Discrete Fourier Transforms*. 2012.

[15] R. D. Cook, D. S. Malkus, M. E. Plesha, and R. J. Witt. *Concepts and Applications of Finite Element Analysis*. 2007.

[16] G. Sadler, F. Fang, J. Kovacs, and K. Irwin. Periodic modification of the Boerdijk-Coxeter helix (tetrahelix). *arXiv preprint arXiv:1302.1174*, pages 1–15, 2013.